 Communications in Theoretical Physics

Commun. Theor. Phys. **72** (2020) 085003 (16pp) https://doi.org/10.1088/1572-9494/ab8a2d

Natural convection of CuO–water nanofluid filled in a partially heated corrugated cavity: KKL model approach

Rizwan Ul Haq[1], Muhammad Usman[2,3] and Ebrahem A Algehyne[3,4]

[1] Department of Electrical Engineering, Bahria University, Islamabad, Pakistan
[2] BIC-ESAT, College of Engineering, Peking University, Beijing 100871, China
[3] State Key Laboratory for Turbulence and Complex Systems, Department of Mechanics and Engineering Science, Peking University, Beijing 100871, China
[4] Department of Mathematics, Faculty of Sciences, University of Tabuk, P. O. Box 741, Tabuk 71491, Saudi Arabia

E-mail: rizwanulhaq.buic@bahria.edu.pk

Received 14 January 2020, revised 13 April 2020
Accepted for publication 15 April 2020
Published 20 July 2020

Abstract

In this article, flow and heat transfer inside a corrugated cavity is analyzed for natural convection with a heated inner obstacle. Thermal performance is analyzed for CuO–water inside a partially heated domain by defining the constraint along the boundaries. For nanofluid analysis, the Koo and Kleinstreuer Li (KKL) model is implemented to deal with the effective thermal conductivity and viscosity. A heated thin rod is placed inside the corrugated cavity and the bottom portion of the corrugated cavity is partially heated. The dimensionless form of nonlinear partial differential equations are obtained through the compatible transformation along with the boundary constraint. The finite element method is executed to acquire the numerical solution of the obtained dimensional system. Streamlines, isotherms and heat transfers are analyzed for the flow field and temperature distribution. The Nusselt number is calculated at the surface of the partially heated domain for various numerical values of emerging parameters by considering the inner obstacle at cold, adiabatic and heated conditions. The computational simulation was performed by introducing various numerical values of emerging parameters. Important and significant results have been attained for temperature and velocities (in both *x*- and *y*-directions) at the vertically and horizontally mean positions of the corrugated duct.

Keywords: heat transfer, nanofluid, finite element method, KKL, corrugated cavity

(Some figures may appear in colour only in the online journal)

1. Introduction

The study of heat transfer analysis is a very attractive area for researchers due to its massive applications in industry, in particular in automobiles, food processing, chemical industries, textile, heating and cooling devices, heavy machinery, etc. Fluid flow and heat transfer are quite complex phenomena within cavities as compared to open surfaces because of their geometrical boundary conditions. Therefore, this area is considered both theoretically and experimentally due to the complex geometry involved. Comprehensive data is available in the literature. Recently, Haq *et al* investigated the heat transfer analysis inside a partially heated trapezoidal cavity [1], a rhombus with fully heated square obstacle [2] and a corrugated cavity [3]. Shape effects of the nanoparticles of forced convection fluid flow inside a semi annulus was studied by Sheikholeslami and Bhatti [4]. Das and Morsi [5] considered a natural convection model inside a dome-shaped cavity. Heat transfer analysis of the natural convection flow of nanofluid enclosed in a quarter-circular shaped cavity was discussed by Uddin *et al* [6]. Oztop *et al* explored the natural convection flow of nanofluid enclosed in an annulus formed by two isothermal cylinders [7] and a rectangle which was partially heated [8]. In another study, thermal and mass performance of fluid under the impact of the Lewis number for the buoyancy ratio parameter through the FEM was analyzed by Rahman *et al* [9]. In that article they investigated the triangular shaped cavity with a sinusoidal bottom wall.

The influence of wavy surface features on natural convection heat transfer in a cosine corrugated square cavity with Cu–H_2O nanofluid was reported by Shirvan *et al* [10]. They observed that the sensitivity of Nu_m to wavy wavelengths is similar to the sensitivity of wavy amplitude while the sensitivity of the Nusselt number is more sensitive to the parameter of A for a low level of effective parameters. Sheikholeslami and Bokni [11] described the magnetohydrodynamics effects on CuO–water due to temperature difference inside a curved domain shell. They used the Koo and Kleinstreuer Li (KKL) model to investigate the significant outcomes of Brownian motion of the particles and applied the lattice Boltzmann method to simulate the proposed model. The influence of various emerging parameters such as Darcy number, Rayleigh number, Hartmann number and nanofluid volume fraction on heat transfer behavior were demonstrated. Recently, a numerical investigation on the conjugate natural convection in a circular pipe comprising water (H_2O) can be found in [12]. Significant contributions regarding wavy-shaped cavities has been presented by numerous authors [13–16].

A mixture of nano-sized particles and a base fluid is known as a nanofluid. Base fluid include water, ethylene glycol, kerosene, engine oil and various other fluids which have poor thermal conductivity. Choi [17] reported that the suspension of nanoparticles inside the abovementioned fluids can enhance the thermal conductivity of the base fluid. Later, his idea was proved by various researchers both experimentally and theoretically. Many comprehensive and qualitative theoretical studies related to the nanofluid domain are available in the literature, but we only include very recent literature in our study. Mohyud-Din *et al* [18] examined the flow of carbon–water nanofluid beside the influence of thermal radiation and Marangoni convection. They reported a least square investigation of the governing flow problem. Usman *et al* [19] analyzed the transportation of heat and fluid flow of water and ethylene glycol-based Cu nanoparticles between two parallel squeezing porous disks. They simulated the problem by means of the least square Galerikin technique. The flow of CuO–H_2O (copper–water) nanofluid and heat transfer enhancement with a melting surface was simulated by Sheikholeslami and Sadoughi [20]. The transport of heat of water-based Cu and Ag (silver) nanoparticles along a converging/diverging channel by means of the least square approach was analyzed by Usman *et al* [21]. Sheikholeslami and Shehzad [22] numerically analyzed the flow of an Fe_3O_4–H_2O nanofluid in permeable media under the influence of an external magnetic source. A detailed analysis was proposed by Usman *et al* [23] for heat and fluid flow of ferrofluids due to constant heat flux along a plate. Recently, Hamid *et al* [24] described the influence of MoS_2 nanoparticles along with the shape factor for nanofluid flow through a moving surface. The Galerkin approach was introduced to handle the mentioned model.

Natural convection phenomena and their mathematical modeling in the form of differential equations are based upon nonlinear terms. Many algorithms have been developed or extended to tackle the complex nature nonlinear physical and mathematical problems. Previously, various numerical, [25, 26], analytical [27–29] and wavelet-based techniques [30, 31] have been adopted to analyze the solutions of the abovementioned problems. A careful literature survey witnesses that advantages and disadvantages of said algorithms are found. The main purpose of the research community is to remove such disadvantages. A numerical algorithm FEM is comparatively better tool to tackle the nonlinear problem in engineering and mathematical physics. Fluid flow, mass transport, structural analysis, electromagnetic potential and heat transfer are the typical problems which could be tackled via the FEM. The solutions of these problems analytically are referred to as boundary value problems for partial differential equations. The system of algebraic equations can be obtained by means of FEM formulation. The referred algorithm is used extensively to find the solution to cavity and complex natural flow problems [1–3, 32, 34, 35].

In the present study, we examined the impact of CuO nanoparticles incorporated with a base fluid inside a corrugated cavity. A rod is placed inside the cavity. The vertical walls are cold, the top surface kept adiabatic and the bottom surface kept partially heated. We used the KKL model [2] for viscosity and effective thermal conductivity. The finite element method (FEM) [1] is proposed and applied effectively to investigate the above model numerically. Streamlines, isotherms and Nusselt numbers are generated to show the fluid flow, temperature and heat transfer varying numerous parameters.

2. Mathematical formulation

Consider the steady, incompressible and laminar flow in a two-dimensional CuO–water nanofluid enclosed in a cavity having a rectangular shape with smooth vertical lines while the bottom and top boundaries are corrugated. A rod is placed inside the cavity as shown in figure 1.

In addition, the vertical walls are cold, the top surface kept adiabatic and the bottom surface kept partially heated. Let U and V represent the velocity components in x- and y-directions, respectively. Taking into account the above assumptions and after applying the Boussinesq approximation, we get the following mathematical model [2]:

$$\frac{\partial u}{\partial x}+\frac{\partial v}{\partial y}=0, \tag{1}$$

$$u\frac{\partial u}{\partial x}+v\frac{\partial u}{\partial y}=-\frac{1}{\rho_{nf}}\frac{\partial p}{\partial x}+\nu_{nf}\left(\frac{\partial^2 u}{\partial x^2}+\frac{\partial^2 u}{\partial y^2}\right), \tag{2}$$

$$u\frac{\partial v}{\partial x}+v\frac{\partial v}{\partial y}=-\frac{1}{\rho_{nf}}\frac{\partial p}{\partial y}+\nu_{nf}\left(\frac{\partial^2 v}{\partial x^2}+\frac{\partial^2 v}{\partial y^2}\right)+g\beta_{nf}(T^{*}-T_c), \tag{3}$$

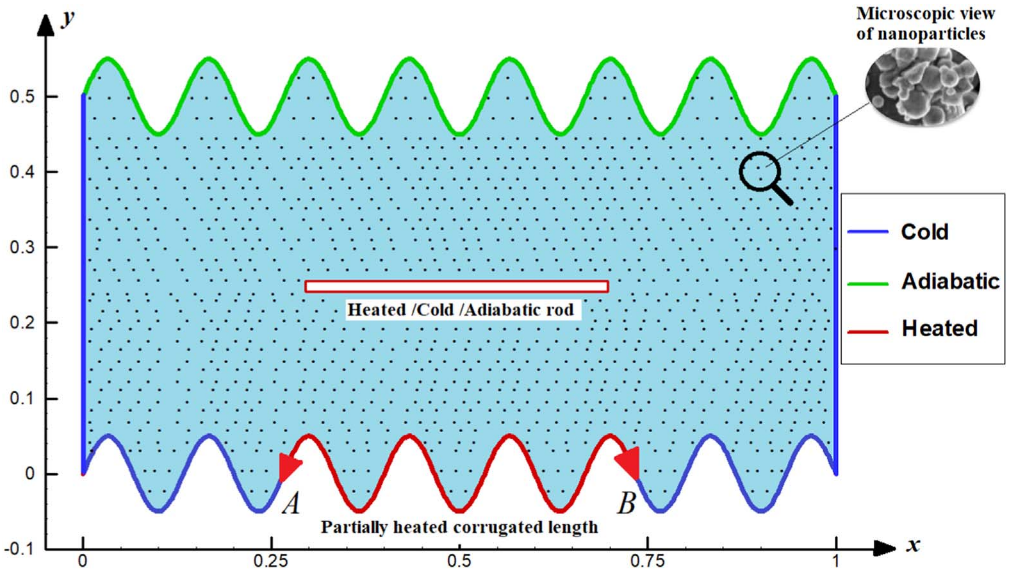

Figure 1. Geometry of the model.

$$(\rho c_p)_{nf}\left(u\frac{\partial T^*}{\partial x}+v\frac{\partial T^*}{\partial y}\right)=k_{nf}\left(\frac{\partial^2 T^*}{\partial x^2}+\frac{\partial^2 T^*}{\partial y^2}\right), \tag{4}$$

associated with the following boundary conditions:

$$\begin{cases} T^*\left(x,\, y=a\sin\left(\frac{n\pi x}{L}\right)\right)=T_c;\ \text{ for } 0\leqslant x\leqslant aL, & \text{Temperature at bottom wall}\\ T^*\left(x,\, y=a\sin\left(\frac{n\pi x}{L}\right)\right)=T_h \text{ for } x=|AB|\,L, & \text{Temperature at bottom wall}\\ T^*\left(x,\, y=a\sin\left(\frac{n\pi x}{L}\right)\right)=T_c;\ \text{ for } bL\leqslant x\leqslant L, & \text{Temperature at bottom wall}\\ \frac{\partial}{\partial y}T^*\left(x,\, y=\frac{L}{2}+a\sin\left(\frac{n\pi x}{L}\right)\right)=0;\ \text{ for } 0\leqslant x\leqslant L, & \text{Temperature at upper wall}\\ T^*(x=0,\, y)=T^*(x=1,\, y)=T_c;\ \text{ for } 0\leqslant y\leqslant \frac{L}{2} & \end{cases},$$

and $u=v=0$ at all walls. In the above equations, the velocity component of the x- and y-directions are represented by u and v. Wavelength number, amplitude, temperature of the fluid, pressure, cold side and partially heated domain are denoted by n, a, T^*, p, T_c and $|AB|$, respectively. Moreover, ν_{nf}, ρ_{nf}, β_{nf}, k_{nf} and $(\rho c_p)_{nf}$ represent the dynamic viscosity, density, coefficient of thermal expansion, thermal conductivity and heat capacity of the nanofluid, respectively, and defined as [2]:

$$\mu_{\text{static}}=\frac{\mu_f}{(1-\phi)^{2.5}},\quad \rho_{nf}=\phi\rho_p+(1-\phi)\rho_f, \tag{5}$$

$$\beta_{nf}=\phi\beta_p+(1-\phi)\beta_f, \tag{6}$$

$$(\rho c_p)_{nf}=\phi(\rho c_p)_p+(1-\phi)(\rho c_p)_f. \tag{7}$$

Here, we used a new expression for the thermal conductivity defined in [2]:

$$k_{nf}=k_{\text{static}}+k_{\text{Brownian}}.$$

The following model has been used to compute the static and Brownian parts:

$$\frac{k_{\text{static}}}{k_f}=1+\frac{3\left(\frac{k_p}{k_f}-1\right)\phi}{\left(\frac{k_p}{k_f}+2\right)-\left(\frac{k_p}{k_f}-1\right)\phi},$$

$$k_{\text{Brownian}}=5.10^4\beta\phi(\rho c_p)_f\sqrt{\frac{\kappa_b T_0}{\rho_p d_p}}f(T_0,\,\phi).$$

Li [33] revised this model and established new relationship function ξ. This new relation is given as follows:

$$k_{\text{Brownian}}=5.10^4\phi(\rho c_p)_f\sqrt{\frac{\kappa_{\text{B}} T_0}{\rho_p d_p}}\,\xi(T_0,\,\phi,\,d_p),$$

Table 1. Thermophysical properties of water and CuO nanoparticles.

Properties →	ρ (kg m^{-3})	C_p (J kg^{-1} K)	k (W m^{-1} K)	$\beta \times 10^5$ (K^{-1})	d_s (nm)
Water	997.1	4179	0.613	21	–
CuO	6500	540	18	29	45

where the Boltzmann constant κ_B is defined as $\kappa_B = 1.38 \times 10^{-23}$J K^{-1} and $T_0 = 0.5(T_h + T_c)$. The additional function ξ is given as:

$$\begin{aligned}\xi(T_0, \phi, d_p) &= (\alpha_1 + \alpha_2 \ln(d_p) + \alpha_3 \ln(\phi) \\ &+ \alpha_4 \ln(d_p)\ln(\phi) + \alpha_5 \ln(d_p)^2)\ln(T_0) \\ &+ (\alpha_6 + \alpha_7 \ln(d_p) + \alpha_8 \ln(\phi) + \alpha_9 \ln(d_p)\ln(d_p) \\ &+ \alpha_{10} \ln(d_p)^2).\end{aligned}$$

In the above, the coefficients $\alpha_i (i = 1 \ldots 10)$ are given in table 2. The numerical values of the thermophysical properties of the nanofluid are defined in table 1. Also, the effective viscosity due to the effects of Brownian motion is given as [33]:

$$\mu_{nf} = \mu_{\text{static}} + \mu_{\text{Brownian}} = \mu_{\text{static}} + \frac{k_{\text{Brownian}}}{k_f} \times \frac{\mu_f}{\Pr_f}.$$

$$A_1\left(U\frac{\partial U}{\partial X} + V\frac{\partial U}{\partial Y}\right) = -\frac{\partial P}{\partial X} + A_2 \Pr\left(\frac{\partial^2 U}{\partial X^2} + \frac{\partial^2 U}{\partial Y^2}\right), \quad (10)$$

$$A_1\left(U\frac{\partial V}{\partial X} + V\frac{\partial V}{\partial Y}\right) = -\frac{\partial P}{\partial Y} + A_2 \Pr\left(\frac{\partial^2 V}{\partial X^2} + \frac{\partial^2 V}{\partial Y^2}\right) + A_3 Ra \Pr T, \quad (11)$$

$$A_4\left(U\frac{\partial T}{\partial X} + V\frac{\partial T}{\partial Y}\right) = A_5\left(\frac{\partial^2 T}{\partial X^2} + \frac{\partial^2 T}{\partial Y^2}\right). \quad (12)$$

The boundary conditions reduce to:

$$\begin{cases} T\left(X, Y = \frac{1}{\lambda}\sin\left(\frac{n\pi X}{L}\right)\right) = 0;\ \text{for } 0 \leqslant X \leqslant a,\ \text{Temperature at bottom wall} \\ T\left(X, Y = \frac{1}{\lambda}\sin\left(\frac{n\pi X}{L}\right)\right) = 1;\ \text{for } X = L_t = |AB|,\ \text{Temperature at bottom wall} \\ T\left(X, Y = \frac{1}{\lambda}\sin\left(\frac{n\pi X}{L}\right)\right) = 0;\ \text{for } b \leqslant X \leqslant 1,\ \text{Temperature at bottom wall} \\ \frac{\partial}{\partial Y}T\left(X, Y = \frac{1}{2} + \frac{1}{\lambda}\sin\left(\frac{n\pi X}{L}\right)\right) = 0;\ \text{for } 0 \leqslant X \leqslant 1,\ \text{Temperature at upper wall} \\ T(X = 0, Y) = T(X = 1, Y) = 0;\ \text{for } 0 \leqslant y \leqslant \frac{1}{2} \end{cases}, \quad (13)$$

Introducing the dimensionless variables to convert equations (1)–(4) into nondimensional form:

$$\begin{aligned}&U = \frac{uL}{\alpha_f},\ V = \frac{vL}{\alpha_f},\ X = \frac{x}{L},\ Y = \frac{y}{L},\ T = \frac{T^* - T_c}{T_h - T_c}, \\ &P = \frac{pL^2}{\rho_f \alpha_f^2},\ \Pr = \frac{\nu_f}{\alpha_f},\ Ra = \frac{g\beta_f(T_h - T_c)L^3}{\alpha_f \nu_f}.\end{aligned} \quad (8)$$

In the above, dimensionless parameter Ra is the Rayleigh number and Pr is the Prandtl number for the base fluid. By means of the above similarity variables system of equations (1)–(4) takes the following form:

$$\frac{\partial U}{\partial X} + \frac{\partial V}{\partial Y} = 0, \quad (9)$$

and $U = V = 0$ at all walls. Here $\lambda = L/a$ represents the amplitude ratio, A_1, A_2, A_3, A_4 and A_5 are introduced just for simplicity. The local Nusselt number is given as:

$$Nu = \int_S \frac{k_{nf}}{k_f}\frac{dT}{dn}dX. \quad (14)$$

$$\begin{aligned}&A_1 = \left(1 - \phi + \frac{\rho_p}{\rho_f}\phi\right),\ A_2 = \left(\frac{1}{(1-\phi)^{2.5}} + \frac{k_{\text{Brownian}}}{k_f \Pr_f}\right), \\ &A_3 = \left(1 - \phi + \frac{(\rho\beta)_p}{(\rho\beta)_f}\phi\right), \\ &A_4 = \left(1 - \phi + \frac{(\rho c_p)_p}{(\rho c_p)_f}\phi\right), \\ &A_5 = \left(1 + \frac{3(k_p - k_f)\phi}{(k_p + 2k_f) - (k_p - k_f)\phi} + \frac{k_{\text{Brownian}}}{k_f}\right).\end{aligned}$$

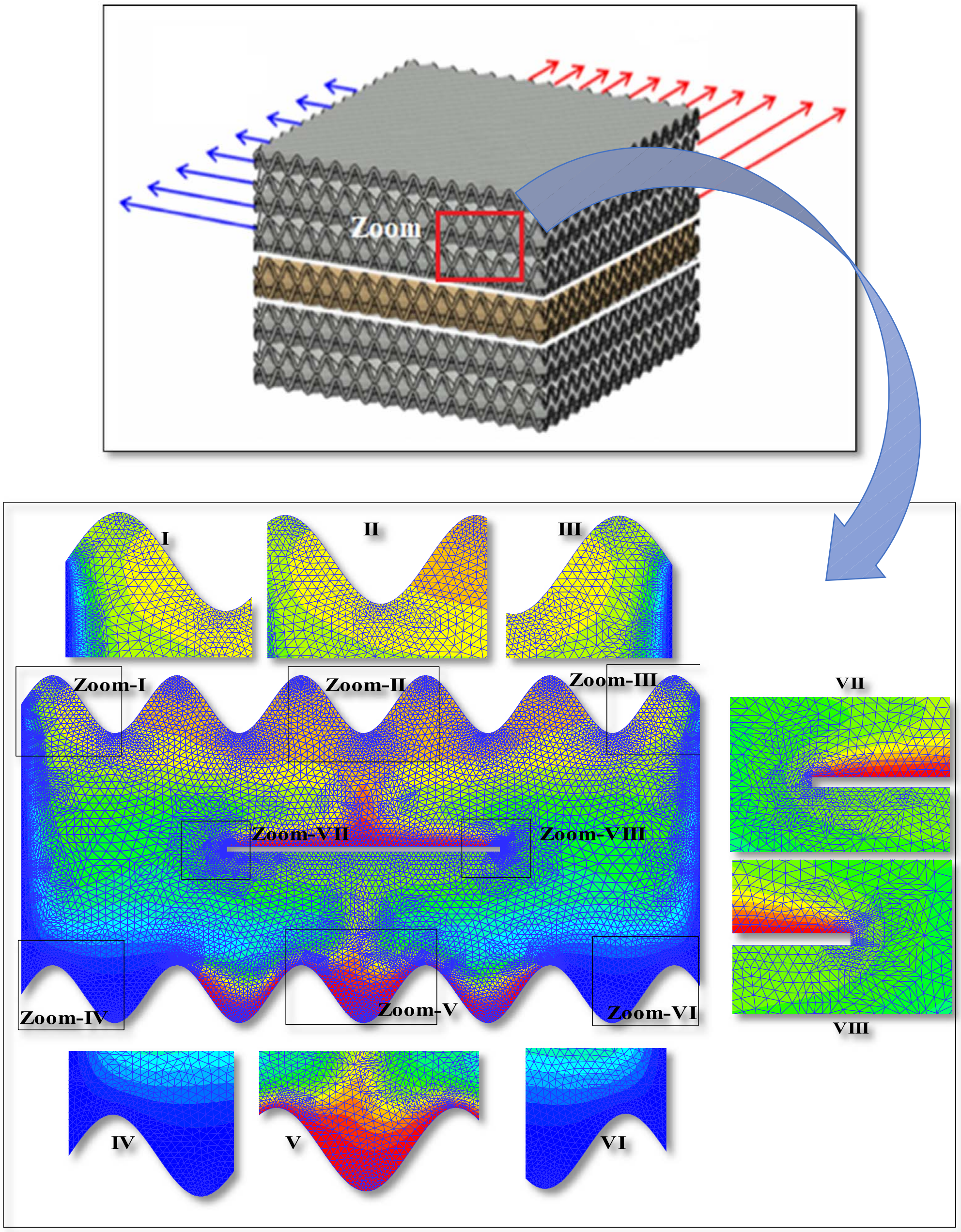

Figure 2. Mesh generation at various corners of the cavity.

3. Solution procedure

The nondimensional forms of dimensionless equations (10)–(12) are highly nonlinear, that is why it is hard to attain the analytical solution. Therefore, the solutions of equations (10)–(12) are analyzed numerically via the Galerkin FEM. To attain the numerical solutions of equations (10)–(12), we ratify penalty the FEM in which pressure term P eliminated by defining the penalty parameter γ, with continuity criteria present in equation (9), therefore we have:

$$P = -\gamma\left[\frac{\partial U}{\partial X} + \frac{\partial V}{\partial Y}\right]. \tag{15}$$

The penalty finite element approach is widely used and a typical approach for the numerical solutions of viscous incompressible fluid. For large values of γ (e.g. 10^7) continuity equation (9) is automatically satisfied. Therefore, by means of equation (15), dimensionless momentum equations (10)–(11) are reduced as:

$$A_1\left(U\frac{\partial U}{\partial X} + V\frac{\partial U}{\partial Y}\right) = -\gamma\frac{\partial}{\partial X}\left[\frac{\partial U}{\partial X} + \frac{\partial V}{\partial Y}\right] + A_2 \mathrm{Pr}\left(\frac{\partial^2 U}{\partial X^2} + \frac{\partial^2 U}{\partial Y^2}\right), \tag{16}$$

Table 2. The coefficient values of nanofluids.

Coefficients a_i	CuO–water	Coefficients a_i	CuO–water
$i = 1$	-26.5933108	$i = 6$	48.40336955
$i = 2$	-0.403818333	$i = 7$	-9.787756683
$i = 3$	-33.3516805	$i = 8$	190.24561009
$i = 4$	-1.915825591	$i = 9$	10.9285386565
$i = 5$	-0.006421858	$i = 10$	-0.72009983664

$$A_1\left(U\frac{\partial V}{\partial X}+V\frac{\partial V}{\partial Y}\right)=-\gamma\frac{\partial}{\partial Y}\left[\frac{\partial U}{\partial X}+\frac{\partial V}{\partial Y}\right]+A_2\,\mathrm{Pr}\left(\frac{\partial^2 V}{\partial X^2}+\frac{\partial^2 V}{\partial Y^2}\right)+RaA_3\,\mathrm{Pr}\,T. \tag{17}$$

In the FEM, we divide the area into a finite number of triangular elements having three nodes. In every element U_i the approximate solution for U in variational formulation is stated as a linear combination of shape function. $\phi_k(x, y)$, $k = 1, 2, 3$ is a linear polynomial. This approximate solution of U concurs with real values at every node of the element. Variational formulation reduces to a matrix equation having order 3 by 3 (stiffness matrix) for unknown local nodal values. Mesh generation at various corners of the cavity is described in figure 2. By means of boundary conditions and inter-element continuity, stiffness matrices are assembled concerning global nodal yields a global matrix equation. For equations (10)–(12), the FEM suggests the following solutions:

$$U=\sum_{i=1}^{N}U_i\phi_i(X, Y),\quad V=\sum_{i=1}^{N}V_i\phi_i(X, Y),\quad T=\sum_{i=1}^{N}T_i\phi_i(X, Y),\ \text{for } 0\leqslant X, Y\leqslant 1. \tag{18}$$

According to the Galerkin FEM, we get the following nonlinear residuals equations for U, V and θ by inserting the above solutions in (12, 16–17) and applying the weak formulation strategy:

$$R_k^U=A_1\sum_{i=1}^{N}U_i\int_\Omega\left[\left(\sum_{i=1}^{N}U_i\phi_i\right)\frac{\partial\phi_i}{\partial X}+\left(\sum_{i=1}^{N}V_i\phi_i\right)\frac{\partial\phi_i}{\partial Y}\right]\times\phi_k\mathrm{d}X\mathrm{d}Y+\gamma\left[\sum_{i=1}^{N}U_i\int_\Omega\frac{\partial\phi_k}{\partial X}\frac{\partial\phi_i}{\partial X}\mathrm{d}X\mathrm{d}Y+\sum_{i=1}^{N}V_i\int_\Omega\frac{\partial\phi_k}{\partial X}\frac{\partial\phi_i}{\partial Y}\mathrm{d}X\mathrm{d}Y\right]+A_2\mathrm{Pr}\sum_{i=1}^{N}U_i\int_\Omega\left[\frac{\partial\phi_k}{\partial X}\frac{\partial\phi_i}{\partial X}+\frac{\partial\phi_k}{\partial Y}\frac{\partial\phi_i}{\partial Y}\right]\mathrm{d}X\mathrm{d}Y, \tag{19}$$

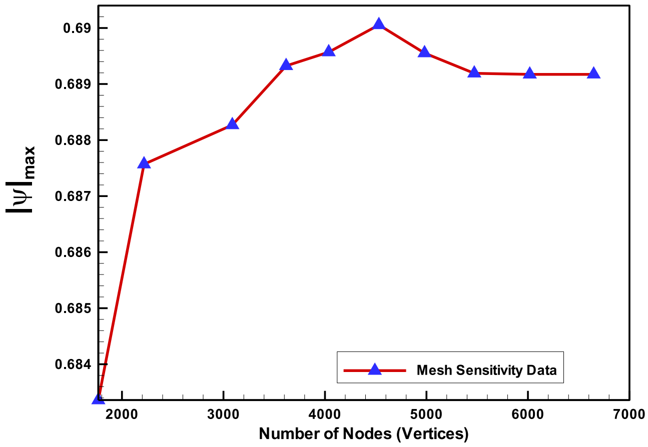

Figure 3. Mesh sensitivity analysis when $Ra = 10^4$, $\phi = 0.2$ and $n = 11$.

$$R_k^V=A_1\sum_{i=1}^{N}V_i\int_\Omega\left[\left(\sum_{i=1}^{N}U_i\phi_i\right)\frac{\partial\phi_i}{\partial X}+\left(\sum_{i=1}^{N}V_i\phi_i\right)\frac{\partial\phi_i}{\partial Y}\right]\phi_k\mathrm{d}X\mathrm{d}Y+\gamma\left[\sum_{i=1}^{N}U_i\int_\Omega\frac{\partial\phi_k}{\partial Y}\frac{\partial\phi_i}{\partial X}\mathrm{d}X\mathrm{d}Y+\sum_{i=1}^{N}V_i\int_\Omega\frac{\partial\phi_k}{\partial Y}\frac{\partial\phi_i}{\partial Y}\mathrm{d}X\mathrm{d}Y\right]+A_2\,\mathrm{Pr}\sum_{i=1}^{N}V_i\int_\Omega\left[\frac{\partial\phi_k}{\partial X}\frac{\partial\phi_i}{\partial X}+\frac{\partial\phi_k}{\partial Y}\frac{\partial\phi_i}{\partial Y}\right]\mathrm{d}X\mathrm{d}Y-A_3Ra\,\mathrm{Pr}\int_\Omega\left(\sum_{i=1}^{N}\theta_i\phi_i\right)\phi_k\mathrm{d}X\mathrm{d}Y, \tag{20}$$

$$R_k^T=A_4\sum_{i=1}^{N}T_i\int_\Omega\left[\left(\sum_{i=1}^{N}U_i\phi_i\right)\frac{\partial\phi_i}{\partial X}+\left(\sum_{i=1}^{N}V_i\phi_i\right)\frac{\partial\phi_i}{\partial Y}\right]\phi_k\mathrm{d}X\mathrm{d}Y+A_5\sum_{i=1}^{N}T_i\int_\Omega\left[\frac{\partial\phi_k}{\partial X}\frac{\partial\phi_i}{\partial X}+\frac{\partial\phi_k}{\partial Y}\frac{\partial\phi_i}{\partial Y}\right]\mathrm{d}X\mathrm{d}Y. \tag{21}$$

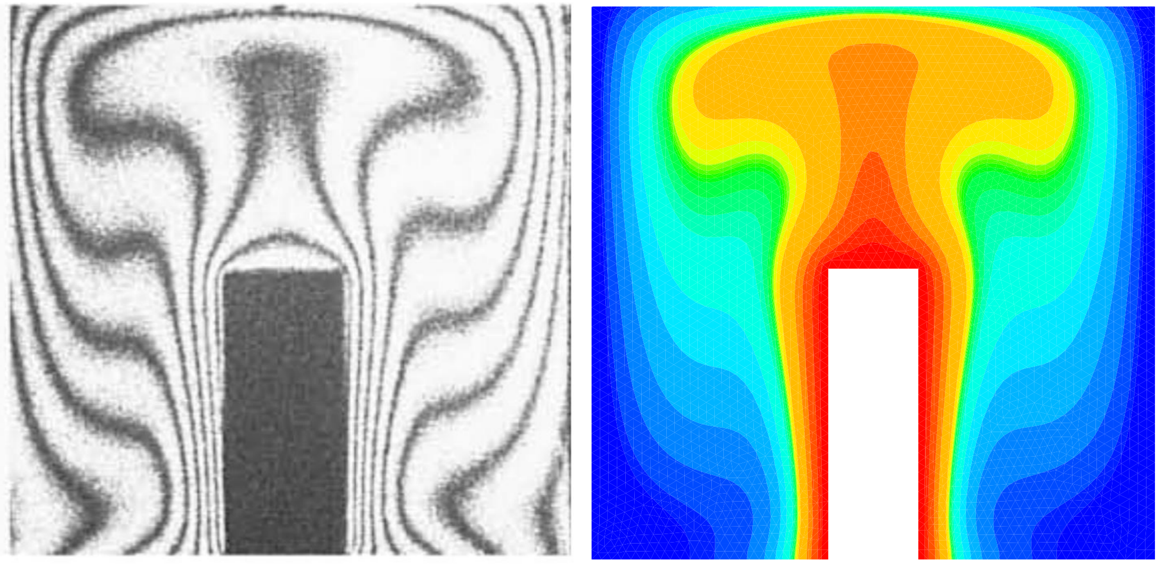

(a) Experimental work [39]. (b) Present work

Figure 4. Variation of isotherm behavior in the comparison with (a) experimental work by Paroncini and Corvaro [39] and (b) present work when $\Pr = 6.2$, $Ra = 1.24 \times 10^5$.

To appraise the integrals of the above residual equations, we use bi-quadratic basis functions along with the three-point Gaussian quadrature, whereas the two-point Gaussian quadrature is used for the term containing penalty terms in equations (19)–(20). The above system reduces to the following matrices form as:

$$[\boldsymbol{A} + \gamma \boldsymbol{B}]\chi = \boldsymbol{C},$$

where, matrices $\boldsymbol{A}$ and $\boldsymbol{B}$ are achieved from the Jacobian of residuals defined in equations (19) and (21). The unknown vector is defined by χ. Due to the large value of γ, the contribution of $\gamma\boldsymbol{B}$ is relatively high compared to $\boldsymbol{A}$. This implies that the current model only endures with continuity equation (9) [35, 36]. The Newton Raphson procedure is adopted to solve the nonlinear residual equations (19)–(21) for the unknowns present in the expressions (18). We obtain the $3N$ by $3N$ system in each iteration of the Newton Raphson procedure

$$\mathcal{J}(\chi^n)[\chi^n - \chi^{n+1}] = \mathcal{R}(\chi^n)$$

is solved. Here $\boldsymbol{J}(\chi^n)$ is the Jacobian matrix [36] and $\boldsymbol{R}(\chi^n)$ is the residuals vector. This iterative procedure is stopped by the given convergence level. Motion of fluid is displayed by means of the stream functions ψ attained for the velocity components U and V and the relation between them is given as [36]:

$$U = \frac{\partial \psi}{\partial Y}, \quad V = -\frac{\partial \psi}{\partial X},$$

which return the following expression:

$$\frac{\partial U}{\partial Y} - \frac{\partial V}{\partial X} = \frac{\partial^2 \psi}{\partial X^2} + \frac{\partial^2 \psi}{\partial Y^2}. \tag{22}$$

Now considering the trial solution for stream function ψ by means of the basis $\{\phi_i\}_{i=1}^N$ which is given as:

$$\psi = \sum_{i=1}^{N} \psi_i \phi(X, Y).$$

Now, by means of the Galerkin FEM, we obtain the following residual equation for equation (22):

$$\begin{aligned} R_k^{\psi} &= \sum_{i=1}^{N} U_i \int_{\Omega} \phi_k \frac{\partial \phi_i}{\partial Y} \mathrm{d}X\,\mathrm{d}Y + \sum_{i=1}^{N} V_i \int_{\Omega} \phi_k \frac{\partial \phi_i}{\partial X} \mathrm{d}X\,\mathrm{d}Y \\ &+ \sum_{i=1}^{N} \psi_i \int_{\Omega} \left[\frac{\partial \phi_k}{\partial X}\frac{\partial \phi_i}{\partial X} + \frac{\partial \phi_k}{\partial Y}\frac{\partial \phi_i}{\partial Y} \right] \mathrm{d}X\,\mathrm{d}Y. \end{aligned} \tag{23}$$

At the boundaries of the nodes, the residual equation (23) stratified $\psi = 0$. Integral of equation (23) evaluated by means of bi-quadratic basis function, consequently unknowns ψ's achieved by solving N linear residual equation (23). The local Nusselt number, tangent to curve $\sin(11\pi X)/20$, along the partially heated corrugated length at $\sin(11\pi X)/20$ and the heated fin/obstacle $Y = 0.255$ are defined as:

Tangent to the curve $Y = \sin(11\pi X)/20$:

$$Nuss|_{Y=0.05} = \int_{L_H} \left(-\frac{\partial \theta}{\partial Y}\right) \mathrm{d}X. \tag{24}$$

Along the partially heated corrugated $Y = \sin(11\pi X)/20$:

$$Nuss|_{Y=\sin(11\pi X)/20} = \int_H \left(-\frac{\partial \theta}{\partial (Y = \sin(11\pi X)/20)}\right) \mathrm{d}X\,. \tag{25}$$

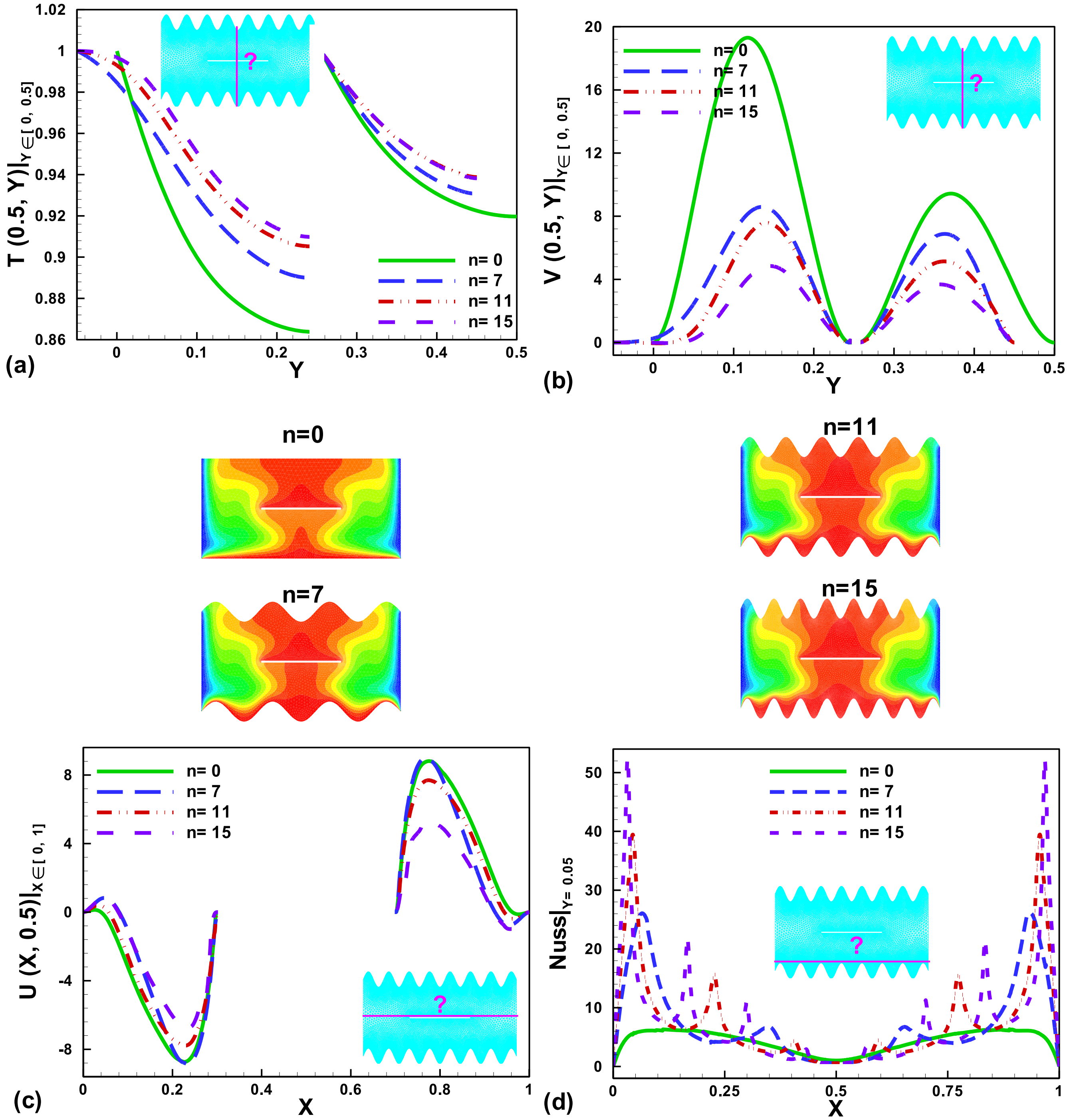

Figure 5. Variation of (a) temperature along the y-direction, (b) velocity V along the y-direction, (c) velocity U along the x-direction, and (d) Nusselt number at $Y = 0.05$ for various values of wavelengths number 'n' when $Ra = 10^5$ and $\phi = 0.2$.

Along the heated fin/obstacle at $Y = 0.255$:

$$Nuss|_{Y=0.255} = \int_{0.3}^{0.7} \left(-\frac{\partial \theta}{\partial Y}\right) \mathrm{d}X. \tag{26}$$

After defining the entire procedure, we have validated our results (see table 3) with the existing literature published by Khanafer *et al* [37] and Davis [38]. It can be seen that our results provide accurate and stable results up to four decimal places.

Figure 3 demonstrated the mesh-sensitive analysis of the current model. We have considered nonuniform mesh unless convergence is not achieved for maximum values of stream function. One can observe in figure 3 that we have run the code 10 times unless the repeated results of maximum values of the stream function is attained. In order to verify the current model with the limiting case of the experimental results by Paroncini and Corvaro [39], an excellent comparison is attained in figure 4 for isotherm variation when $\mathrm{Pr} = 6.2$, $Ra = 1.24 \times 10^5$.

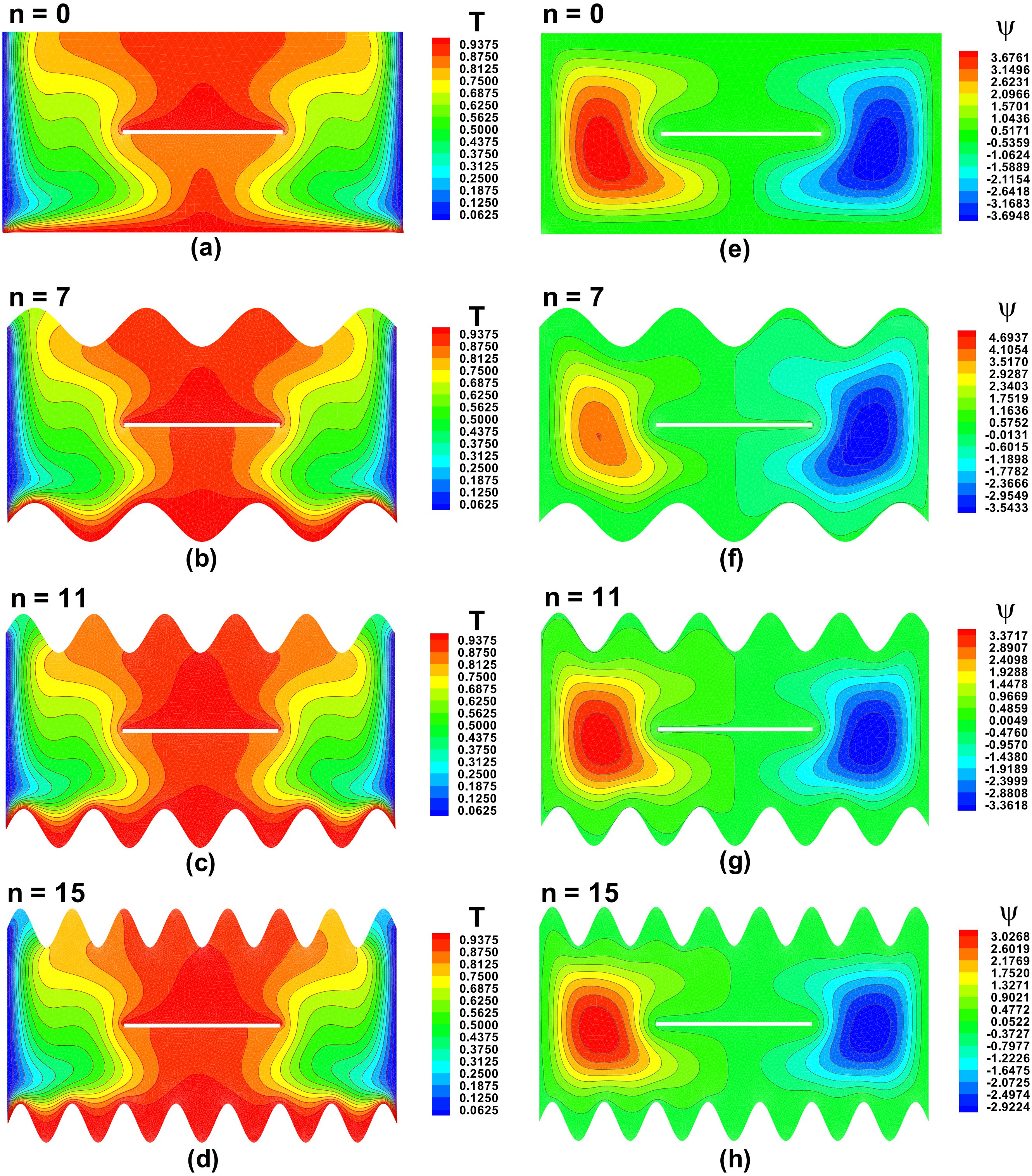

Figure 6. Variation of (a)–(d) isotherms and (e)–(h) stream function for various values of wavelengths number 'n' when $Ra = 10^5$ and $\phi = 0.2$.

4. Results and discussion

In the previous section numerical solutions of heat transfer of CuO–water filled in a corrugated duct with inside a adiabatic rod achieved by means of the Galerkin FEM. This section is devoted to a comprehensive discussion about the effects of different values of Rayleigh number ($10^4 \leqslant Ra \leqslant 10^7$), wavelength ($0 \leqslant n \leqslant 15$), bottom heated portion ($0.18 \leqslant L_T \leqslant 1$), heated conditions at rod (cold, adiabatic and hot) and nanoparticle volume fraction ($0 \leqslant \phi \leqslant 0.2$), on streams lines, isotherms, velocities (U and V) and temperature (T). The Nusselt number measures the rate of heat transfer, that is

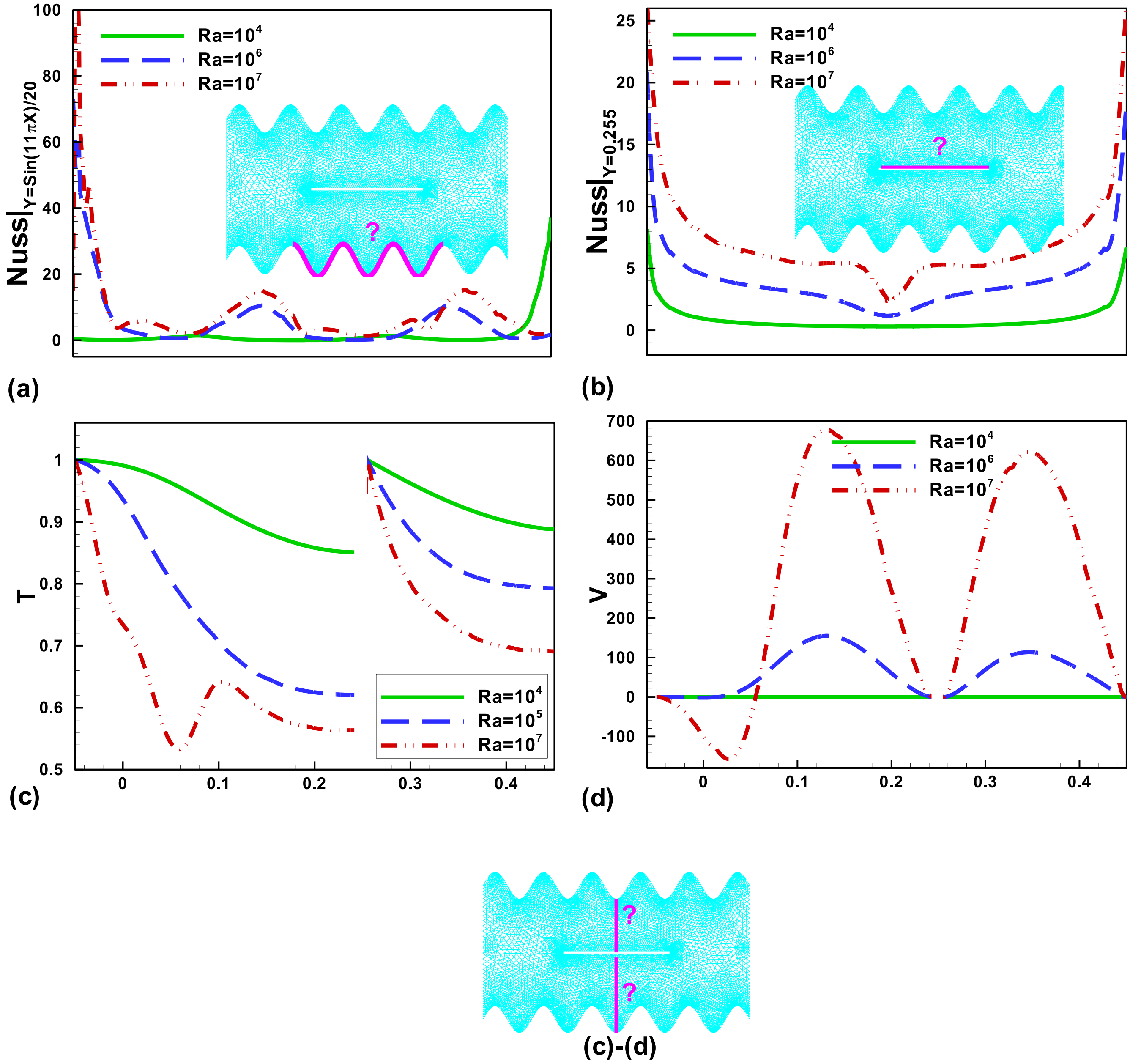

Figure 7. Variation of (a) Nusselt number at $Y = \sin\left(\frac{11X}{20}\right)$, (b) Nusselt number at $Y = 0.255$ at inner heated rod, (c) temperature along the y-direction, (d) velocity V along the y-direction for various values of Ra when $n = 11$ and $\phi = 0.2$.

why behavior of the nondimensional Nusselt number due to the variation of various parameters is also considered. Numerical values of thermophysical properties are defined in tables 1 and 2.

Figures 5 and 6 are plotted to analyze the behavior of isotherms and streamlines due to the variation in wavelength parameter. Effects of wavelength parameter on temperature along the y-direction, velocity (V) along the y-direction, velocity (U) along x-direction and Nusselt number. Figure 5(a) represents that temperature enhances and increasing the value of wavelength parameter. It can be seen from figures 5(b), (c) that the velocity (V) along the y-direction increases as the wavelength parameter varies. It is observed that the velocity profile is dominant when the boundary is not corrugated ($n = 0$). Velocity (U) along the x-direction demonstrates the increasing and decreasing behavior when $x \in [0, 0.3)$ and $x \in (0.7, 1]$ of the cavity. As the wavelength increases, the behavior of velocity U increases in the left portion of the cavity and decreases in the right portion. The effects of wavelength parameter on heat transfer rate are portrayed figure 5(d). This figure shows that heat transfer increases as the wavelength parameter increases. Moreover, it is observed that at vertical walls of the cavity, the heat transfer rate is maximum. Physically, this is expected

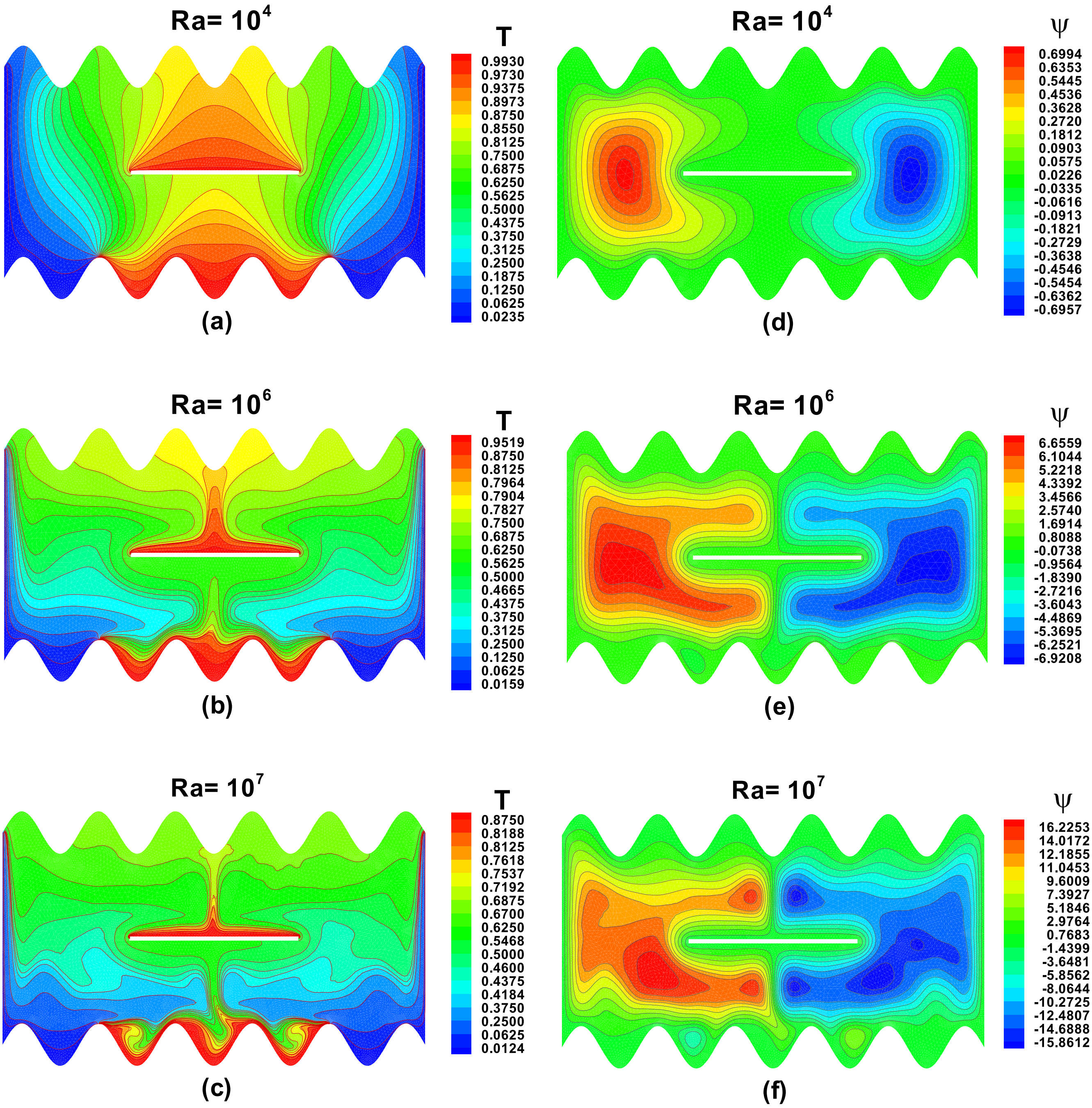

Figure 8. Variation of (a)–(c) isotherms and (d)–(f) stream function with respect to various values of Ra when $n = 11$ and $\phi = 0.2$.

since the vertical walls are set to be cold. Figures 6(a)–(d) show the heat distribution against the variation in wavelength parameter. As it is enhanced, the value of wavelength parameter heat is distributed more to nearby areas. This phenomenon is well supported in figure 5(a). Due to the cold vertical wall, temperature distribution begins to grow from the center of the cavity in the direction of upper wall. Figures 5(e)–(h) disclose the impact of wavelength parameter on fluid flow. Fluid flow becomes stronger as upsurges the value of wavelength parameter occur. Further, it is observed that as wavelength parameter increases, the streamlines reach the full cavity.

The effect of Rayleigh number on isotherms, streamlines, Nusselt number, temperature along y-direction and velocity (V) along y-direction is portrayed in figures 7 and 8 at prescribed paths. Figures 7(a), (b) shows that as the Rayleigh number increases, the heat transfer rate upsurges gradually. It is seen that at vertical walls of the cavity, the heat transfer rate is maximum because the vertical walls are cold. Figure 7(c) demonstrates the effect of Rayleigh number on temperature

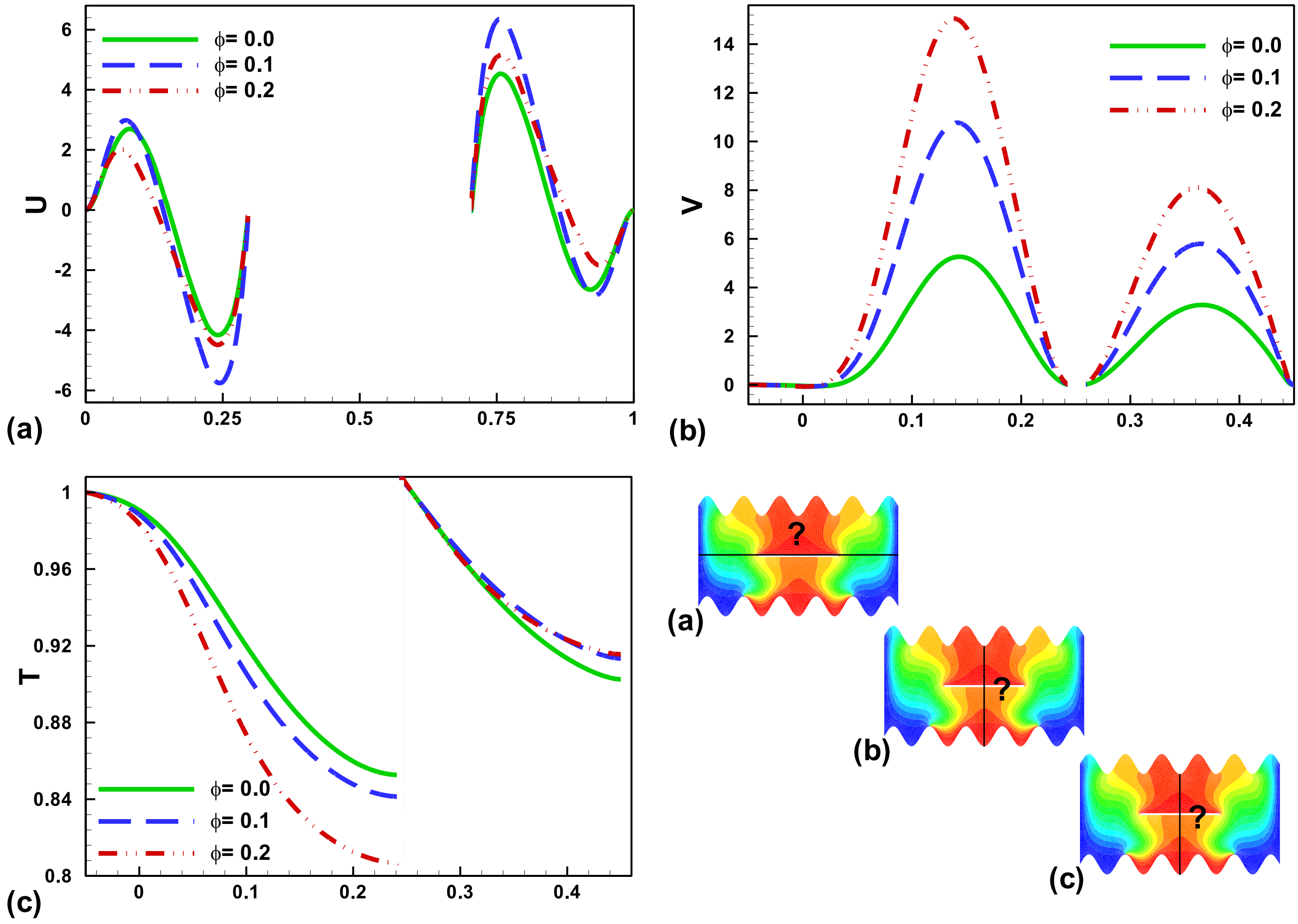

Figure 9. Variation of (a) temperature along the y-direction, (b) velocity V along the y-direction, (c) velocity U along the x-direction for various values of ϕ when $Ra = 10^5$ and $n = 11$.

distribution. Temperature distribution decreases along the vertical mean path and increases Rayleigh number. As Rayleigh number increases velocity (V) along the y-direction due to the variation in Rayleigh number can be seen in figure 7(d). Overall behavior of velocity is increasing as upsurges Rayleigh number expect lower half section of the cavity. Figures 8(a)–(c) reveal the behavior of isotherms for different values of Rayleigh number. Clearly, it is observed that increase in Rayleigh number tends to increase in temperature distribution in the cavity. Again, as the results of cold vertical walls temperature distribution begins to grow from the center of the cavity in the direction of upper wall. Impact of fluid flow under the variation of Rayleigh number characterized in figures 8(d)–(f). This figure evident that as growing the values of Rayleigh number, fluid flow become stronger.

The nature of isotherms and streamlines, temperature along y-direction, velocity (V) along y-direction and velocity (U) along x-direction by rising the value of nanoparticles volume fraction is depicted in figures 9–10 along defined paths. Change in velocity (U) along the x-direction by increasing the value of nanoparticles volume fraction displayed in figure 9(a). It can be observed that as enlarges nanoparticles volume fraction velocity decreases near the wall

Table 3. Comparison between present results and other works for the average Nusselt number (Nu_{avg}).

Ra	Present work	Khanafer *et al* [37]	De Vahl Davis [38]
10^3	1.1307	1.118	1.118
10^4	2.2674	2.245	2.243
10^5	4.5851	4.522	4.519
10^6	8.8341	8.826	8.799

of cavity between (0, 0.245) to (0.3, 0.245) and increases near the wall of cavity between (0.7, 0.245) to (1, 0.245). Figure 9(c) illustrate the variation in velocity (V) along y-direction under the influence of nanoparticles volume fraction. As enhancing nanoparticles volume fraction velocity profile increase between (0.5, −0.05) to (0.5, 0.24) and (0.5, 0.25) to (0.5, 0.45). Figure 9(c) exhibit the nature of temperature distribution. Clearly, temperature distribution exhibits the decreasing and increasing behavior between (0.5, −0.05) to (0.5, 0.24) and (0.5, 0.25) to (0.5, 0.45) respectively. Figures 10(a)–(c) display the impact of nanoparticles volume fraction on temperature distribution. Temperature distribution increases as nanoparticles volume fraction increases. Physically this is correct, since temperature increases as the thermal

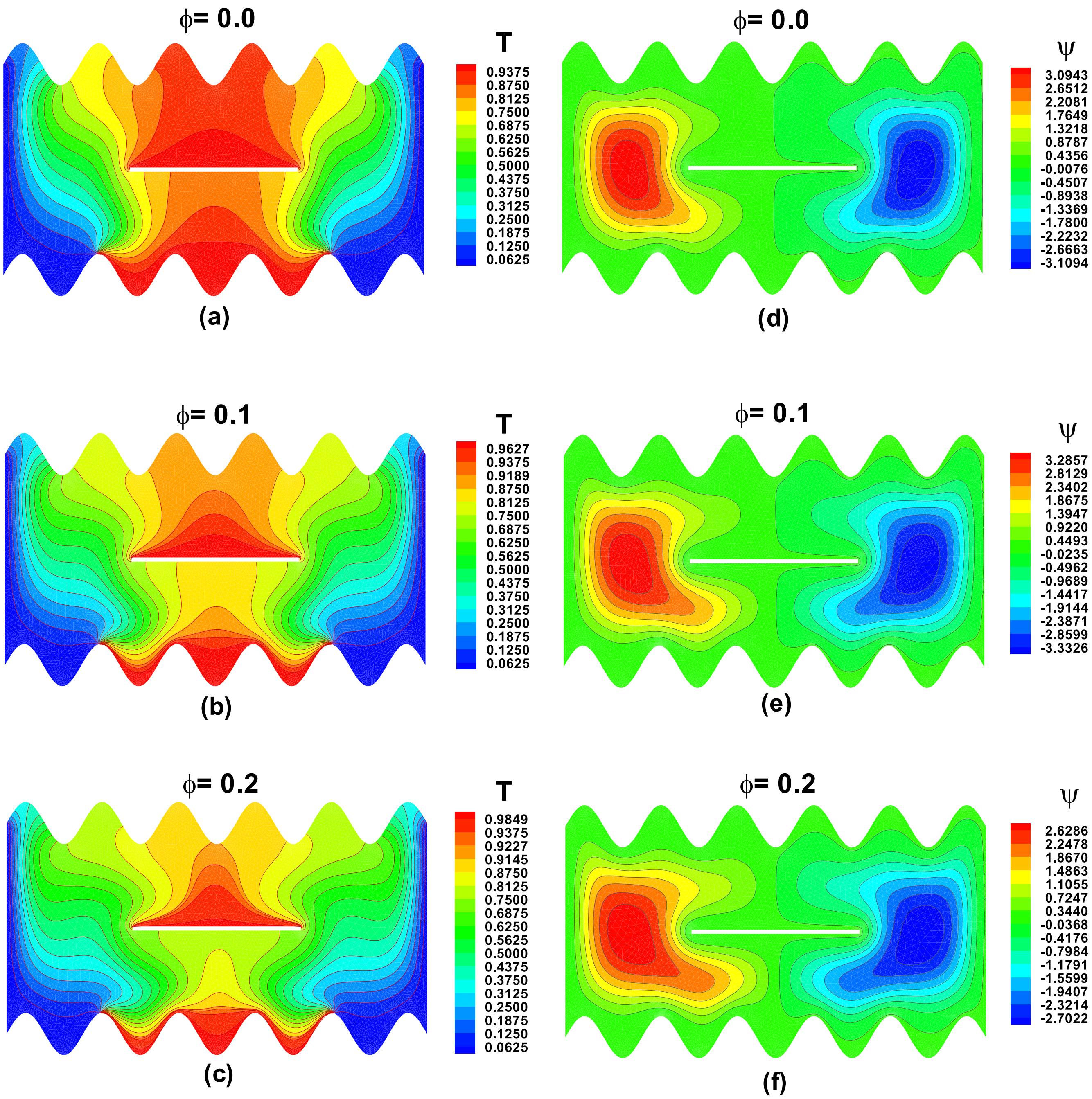

Figure 10. Variation of (a)–(c) isotherms and (d)–(f) stream function for various values of ϕ when $Ra = 10^5$ and $n = 11$.

conductivity property of nanoparticles rises. On the other hand, the streamline behavior for different values of nanoparticle volume fraction is verified in figures 10(d)–(f). This figure shows that by increasing the nanoparticles volume fraction the strength of the molecules is increased, and friction is produced among the particles that effect the stream function.

Figure 11 analyzes the nature of streamlines and isotherms as changing the length of the heated portion 'L_T'. Figures 11(a)–(c) confirm the behavior of temperature distribution under the influence of L_T. It is evident that as it increases the heated portion temperature distribution increases in the cavity. On the other hand, figures 11(d)–(f) interpret the nature of trajectories of fluid motion. It is observed that L_T rises, the trajectories of fluid motion become stronger.

Effects of Rayleigh number on isotherms and streamlines when the inner rod is cold is shown in figure 12. In figures 12(a)–(c) the behavior of temperature distribution under the inspiration of the Rayleigh number is depicted. Temperature of the fluid increases in the cavity the Rayleigh number is enhanced. Figures 12(d)–(f) depict the nature of the fluid trajectories with respect to Rayleigh number. It is noticed that the Rayleigh number increases, the trajectories of the fluid motion become stronger.

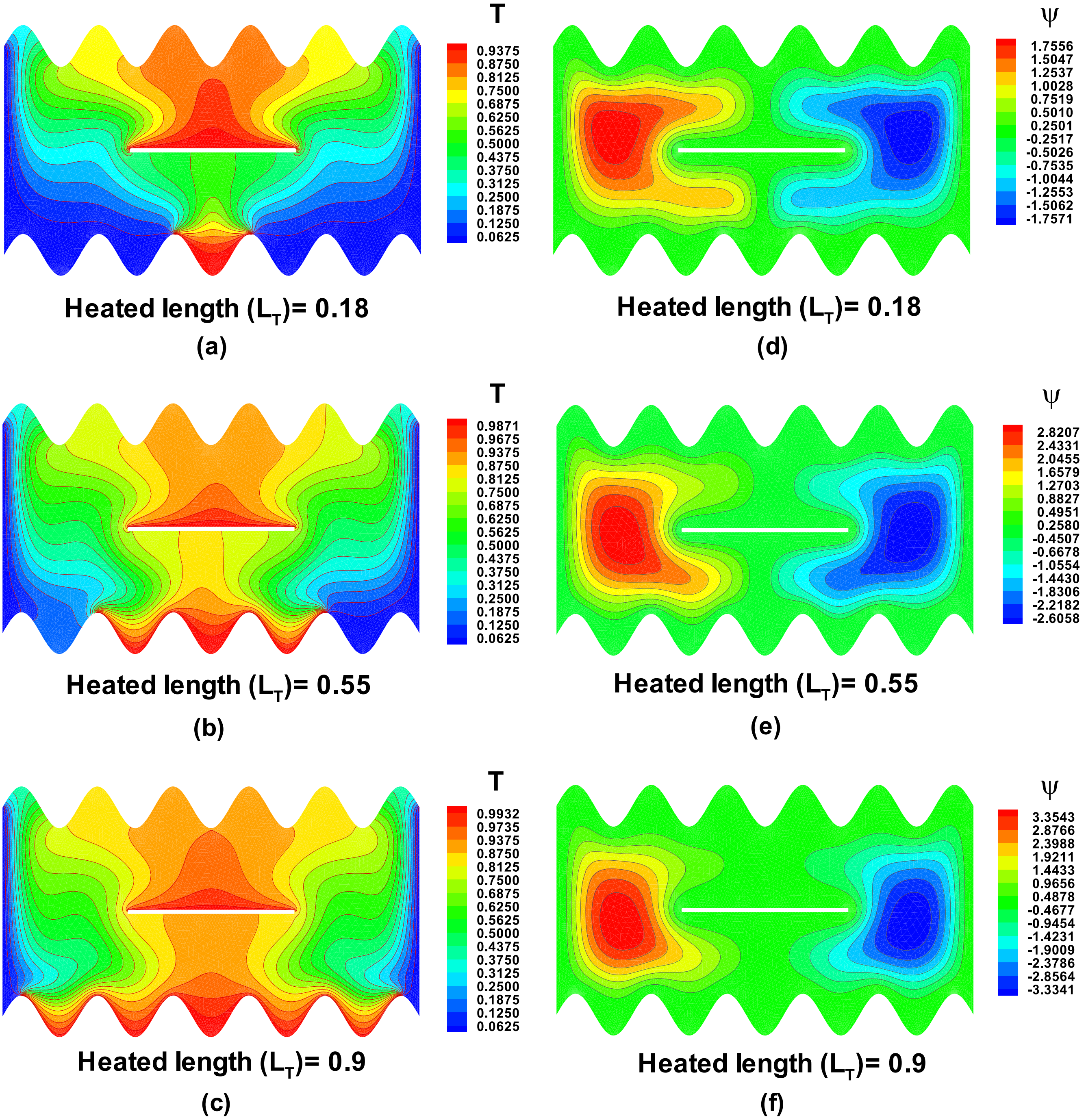

Figure 11. Variation of (a)–(c) isotherms and (d)–(f) stream function for various heated lengths when $\phi = 0.2$, $Ra = 10^5$ and $n = 11$.

5. Conclusion

In this paper, we considered the heat transfer of CuO–water inside a corrugated cavity having bottom wall that is partially heated with an adiabatic rod. Convenient similarity variables are introduced to obtain the nondimensionalized form of the modeled problem. The finite element method is adopted for the numerical solutions of the nondimensionalized system of partial differential equations. Major findings are stated below:

- Temperature distribution, streamlines and heat transfer rate are significantly increased when the wavelength parameter increases.
- By increasing the Rayleigh number, the temperature distribution and streamlines increase gradually.
- An increase in nanoparticle volume fraction causes increments in temperature distribution and trajectories of fluid flow.
- The corrugated surface demonstrates the significant heat transfer within the entire domain of the cavity.

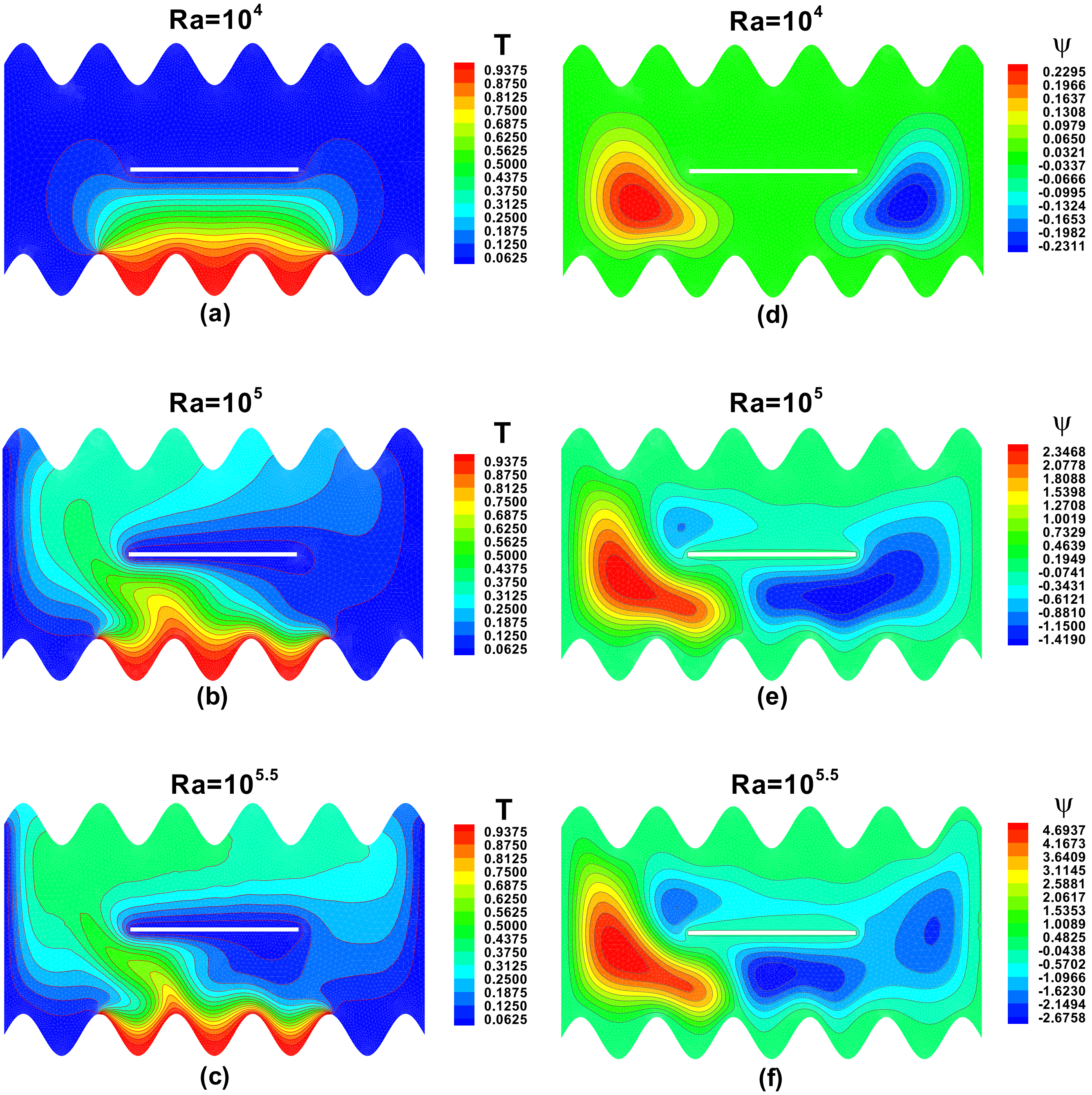

Figure 12. Variation of (a)–(c) isotherms and (d)–(f) stream function with respect to the variation of Ra when the inner rod is cold for $\phi = 0.2,\ Ra = 10^5$ and $n = 11$.

- Isotherms and streamlines become stronger as we increase the length of the heated portion of the cavity.

Acknowledgments

The authors gratefully acknowledge the support given by the University of Tabuk, Ministry of Education in Saudi Arabia.

ORCID iDs

Rizwan Ul Haq https://orcid.org/0000-0002-4595-396X

References

[1] Haq R U, Kazmi S N and Mekkaoui T 2017 Thermal management of water based SWCNTs enclosed in a partially heated trapezoidal cavity via FEM *Int. J. Heat Mass Transfer* **112** 972–82

[2] Haq R U, Soomro F A and Hammouch Z 2018 Heat transfer analysis of CuO-water enclosed in a partially heated rhombus with heated square obstacle *Int. J. Heat Mass Transfer* **118** 773–84

[3] Haq R U, Soomro F A, Mekkaoui T and Al-Mdallal Q M 2018 MHD natural convection flow enclosure in a corrugated cavity filled with a porous medium *Int. J. Heat Mass Transfer* **121** 1168–78

[4] Sheikholeslami M and Bhatti M M 2017 Forced convection of nanofluid in presence of constant magnetic field considering shape effects of nanoparticles *Int. J. Heat Mass Transfer* **111** 1039–49

[5] Das S and Morsi Y 2002 Natural convection inside dome shaped enclosures *Int. J. Numer. Methods Heat Fluid Flow* **12** 126–41

[6] Uddin M J, Alam M S and Rahman M M 2017 Natural convective heat transfer flow of nanofluids inside a quarter-circular enclosure using nonhomogeneous dynamic model *Arab. J. Sci. Eng.* **42** 1883–901

[7] Selimefendigil F and Öztop H F 2017 Conjugate natural convection in a nanofluid filled partitioned horizontal annulus formed by two isothermal cylinder surfaces under magnetic field *Int. J. Heat Mass Transfer* **108** 156–71

[8] Oztop H F and Abu-Nada E 2008 Numerical study of natural convection in partially heated rectangular enclosures filled with nanofluids *Int. J. Heat Fluid Flow* **29** 1326–36

[9] Rahman M M, Öztop H F, Ahsan A and Orfi J 2012 Natural convection effects on heat and mass transfer in a curvilinear triangular cavity *Int. J. Heat Mass Transfer* **55** 6250–9

[10] Shirvan K M, Ellahi R, Mamourian M and Moghiman M 2017 Effects of wavy surface characteristics on natural convection heat transfer in a cosine corrugated square cavity filled with nanofluid *Int. J. Heat Mass Transfer* **107** 1110–8

[11] Sheikholeslami M and Rokni H B 2017 Free convection of CuO–H_2O nanofluid in a curved porous enclosure using mesoscopic approach *Int. J. Hydrogen Energy* **42** 14942–9

[12] Choi M Y and Choi H G 2017 A numerical study on the conjugate natural convection in a circular pipe containing water *J. Mech. Sci. Technol.* **31** 3261–9

[13] Shenoy A, Sheremet M and Pop I 2019 *Convective Flow and Heat Transfer from Wavy Surfaces: Viscous Fluids, Porous Media, and Nanofluids* 1st edn (Boca Raton, FL: CRC Press)

[14] Sheremet M, Pop I, Öztop H F and Abu-Hamdeh N 2017 Natural convection of nanofluid inside a wavy cavity with a non-uniform heating: entropy generation analysis *Int. J. Numer. Methods Heat Fluid Flow* **27** 958–80

[15] Sheremet M A, Revnic C and Pop I 2017 Free convection in a porous wavy cavity filled with a nanofluid using Buongiorno's mathematical model with thermal dispersion effect *Appl. Math. Comput.* **299** 1–15

[16] Sheikholeslami M, Sheremet M A, Shafee A and Li Z 2019 CVFEM approach for EHD flow of nanofluid through porous medium within a wavy chamber under the impacts of radiation and moving walls *J. Therm. Anal. Calorim.* **138** 573–81

[17] Choi S 1995 Enhancing thermal conductivity of fluids with nanoparticles *FED* **231** 99–103

[18] Mohyud-Din S T, Usman M, Afaq K, Hamid M and Wang W 2017 Examination of carbon-water nanofluid flow with thermal radiation under the effect of Marangoni convection *Eng. Comput.* **34** 2330–43

[19] Usman M, Hamid M, Haq R U and Wang W 2018 Heat and fluid flow of water and ethylene-glycol based Cu-nanoparticles between two parallel squeezing porous disks: LSGM approach *Int. J. Heat Mass Transfer* **123** 888–95

[20] Sheikholeslami M and Sadoughi M K 2018 Simulation of CuO-water nanofluid heat transfer enhancement in presence of melting surface *Int. J. Heat Mass Transfer* **116** 909–19

[21] Usman M, Haq R U, Hamid M and Wang W 2018 Least square study of heat transfer of water based Cu and Ag nanoparticles along a converging/diverging channel *J. Mol. Liq.* **249** 856–67

[22] Sheikholeslami M and Shehzad S A 2018 Numerical analysis of Fe_3O_4–H_2O nanofluid flow in permeable media under the effect of external magnetic source *Int. J. Heat Mass Transfer* **118** 182–92

[23] Usman M, Hamid M, Mohyud-Din S T, Waheed A and Wang W 2018 Exploration of uniform heat flux on the flow and heat transportation of ferrofluids along a smooth plate: comparative investigation *Int. J. Biomathematics* **11** 1850048

[24] Hamid M, Usman M, Zubair T, Haq R U and Wang W 2018 Shape effects of MoS_2 nanoparticles on rotating flow of nanofluid along a stretching surface with variable thermal conductivity: a Galerkin approach *Int. J. Heat Mass Transfer* **124** 706–14

[25] Usman M, Haq R U, Hamid M and Wang W 2018 Least square study of heat transfer of water based Cu and Ag nanoparticles along a converging/diverging channel *In J. Mol. Liq.* **249** 856–67

[26] Mehmood R, Rana S and Nadeem S 2018 Transverse thermopherotic MHD oldroyd-B fluid with newtonian heating *Res. Phys.* **8** 686–693

[27] Rashid I, Haq R U, Khan Z H and Al-Mdallal Q M 2017 Flow of water based alumina and copper nanoparticles along a moving surface with variable temperature *J. Mol. Liq.* **246** 354–62

[28] Hamid M, Usman M, Zubair T and Mohyud-Din S T 2017 Comparison of Lagrange multipliers for telegraph equations *Ain Shams Eng. J.* **9** 2323–8

[29] Mohyud-Din S T, Usman M, Wang W and Hamid M 2017 A study of heat transfer analysis for squeezing flow of a Casson fluid via differential transform method *Neural Comput. Appl.* **30** 3253–64

[30] Usman M, Zubair T, Hamid M, Haq R U and Wang W 2018 Wavelets solution of MHD 3D fluid flow in the presence of slip and thermal radiation effects *Phys. Fluids* **30** 023104

[31] Mohyud-Din S T, Zubair T, Usman M and Hamid M 2018 Investigation of heat and mass transfer under the influence of variable diffusion coefficient and thermal conductivity *Indian J. Phys.* (https://doi.org/10.1007/s12648-018-1196-2)

[32] Sheikholeslami M 2017 Magnetic field influence on nanofluid thermal radiation in a cavity with tilted elliptic inner cylinder *J. Mol. Liq.* **229** 137–47

[33] Li J 2008 Computational analysis of nanofluid flow in micro channels with applications to micro heat sink and bio-MEMS *PhD Thesis* North Carolina State University

[34] Junemoo K and Kleinstreuer C 2004 Laminar nanofluid flow in microheatsinks *Int. J. Heat Mass Transfer* **48** 2652–61

[35] Li Z, Sheikholeslami M, Shafee A, Haq R ul, Khan I, Tlili I and Kandasamy R 2019 Solidification process through a solar energy storage enclosure using various sizes of Al2O3 nanoparticles *J. Mol. Liq.* **275** 941–54

[36] Reddy J N 1993 *An Introduction to the Finite Element Method* (New York: McGraw-Hill)

[37] Khanafer K, Vafai K and Lightstone M 2003 Buoyancy-driven heat transfer enhancement in a two dimensional enclosure utilizing nanofluids *Int. J. Heat Mass Transfer* **46** 3639–53

[38] De Vahl Davis G 1962 Natural convection of air in a square cavity, a benchmark numerical solution *Int. J. Numer. Methods Fluids* **3** 249–64

[39] Paroncini M and Corvaro F 2009 Natural convection in a square enclosure with a hot source *Int. J. Therm. Sci.* **48** 1683–95